



OPEN

Magnetic critical behavior of the van der Waals Fe_5GeTe_2 crystal with near room temperature ferromagnetism

Zhengxian Li^{1,2,3}, Wei Xia^{1,2,3}, Hao Su^{1,2,3}, Zhenhai Yu¹, Yunpeng Fu¹, Leiming Chen⁴✉, Xia Wang^{1,5}, Na Yu^{1,5}, Zhiqiang Zou^{1,5} & Yanfeng Guo¹✉

The van der Waals ferromagnet Fe_5GeTe_2 has a Curie temperature T_C of about 270 K, which is tunable through controlling the Fe deficiency content and can even reach above room temperature. To achieve insights into its ferromagnetic exchange that gives the high T_C , the critical behavior has been investigated by measuring the magnetization in Fe_5GeTe_2 crystal around the ferromagnetic ordering temperature. The analysis of the measured magnetization by using various techniques harmonically reached to a set of reliable critical exponents with $T_C = 273.7$ K, $\beta = 0.3457 \pm 0.001$, $\gamma = 1.40617 \pm 0.003$, and $\delta = 5.021 \pm 0.001$. By comparing these critical exponents with those predicted by various models, it seems that the magnetic properties of Fe_5GeTe_2 could be interpreted by a three-dimensional magnetic exchange with the exchange distance decaying as $J(r) \approx r^{-4.916}$, close to that of a three-dimensional Heisenberg model with long-range magnetic coupling.

A prominent virtue of the quasi-two-dimensional (2D) van der Waals (vdW) bonded materials is that they could be exfoliated into multi- or single layer, thus making them useful in various novel heterostructures and devices. Moreover, the vdW materials in the 2D limit exhibit extraordinary physical properties, such as those observed in the intensively studied graphene and transition metal dichalcogenides^{1–6}, etc. Known as the Merin-Wagner theorem⁷, intrinsic long-range magnetic order can not appear in the isotropic magnetic 2D limit because the strong thermal fluctuations in such case prohibit the spontaneous symmetry breaking and hence the long-range magnetic ordering. Nevertheless, a small anisotropy is sufficient to open up a sizable gap in the magnon spectra and consequently stabilizes the magnetic order against finite temperature. This picture has been realized by the observation of long-range ferromagnetic (FM) order in mono- or few-layer CrI_3 ⁸, $\text{Cr}_2\text{Ge}_2\text{Te}_6$ ⁹, $\text{Cr}_2\text{Si}_2\text{Te}_6$ ¹⁰, VSe_2 ¹¹, and MnSe_2 ¹², etc. The vdW magnets in the 2D limit host rich magneto-electrical, magneto-optical, or spin-lattice coupling effects that are capable of producing intriguing properties which are scarcely observed in bulk. Very recently, current-induced magnetic switch was observed in the few-layer Fe_3GeTe_2 ¹³, demonstrating the vdW magnets a versatile platform for nanoelectronics. Moreover, heterostructures constructed by using vdW magnets have profound valleytronics and spintronics device applications^{14,15}. For example, the tunneling magnetoresistance (MR) in spin-filter magnetic vdW CrI_3 heterostructures even approaches $1.9 \times 10^4\%$, remarkably superior to that constructed by using conventional magnetic thin films¹⁶. The easy exfoliation, weak interlayer coupling, and tunability of magnetic properties make the vdW magnets a model family of materials for exploring exotic phenomena and finding novel applications.

In the handful FM vdW magnets, the physical properties in the 2D limit differ from each other due to rather complex magnetic interactions. The semiconducting monolayer CrI_3 is an Ising ferromagnet with very low Curie temperature (T_C) of about 45 K due to the weak superexchange interaction along the Cr-I-Cr pathway^{8,17}. The similar weak FM superexchange in the Heisenberg magnet bilayer $\text{Cr}_2\text{Ge}_2\text{Te}_3$ also results in a low T_C of ~ 30 K,

¹School of Physical Science and Technology, ShanghaiTech University, Shanghai 201210, China. ²Shanghai Institute of Optics and Fine Mechanics, Chinese Academy of Sciences, Shanghai 201800, China. ³University of Chinese Academy of Sciences, Beijing 100049, China. ⁴School of Materials Science and Engineering, Henan Key Laboratory of Aeronautic Materials and Application Technology, Zhengzhou University of Aeronautics, Zhengzhou 450046, Henan, China. ⁵Analytical Instrumentation Center, School of Physical Science and Technology, ShanghaiTech University, Shanghai 201210, China. ✉email: lmchen@zua.edu.cn; guoyf@shanghaitech.edu.cn

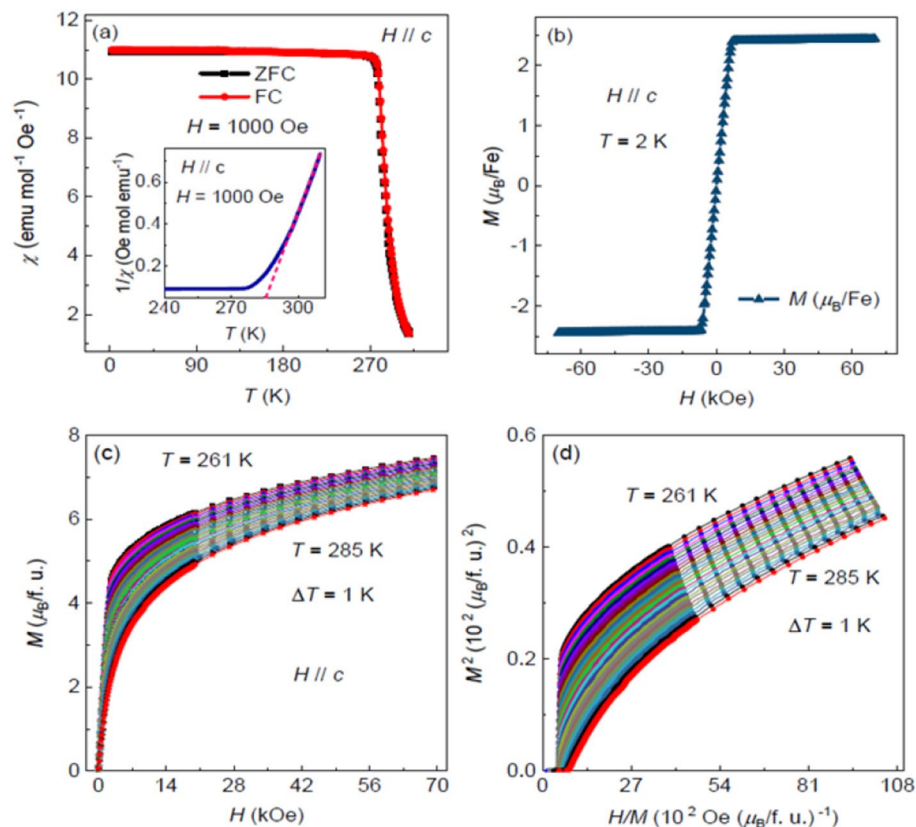


Figure 1. (a) Temperature dependence of magnetization $M(T)$ for Fe_3GeTe_2 under $H = 1$ kOe. The inset shows the inverse susceptibility plotted against temperature and the straight dotted line is Curie–Weiss law fitting. (b) Isothermal magnetization $M(H)$ measured at 2 K. (c) Typical initial magnetization $M(H)$ curves measured from 261 to 285 K with an interval of 1 K. (d) Arrott plots in the form of M^2 vs. H/M (mean field model) around T_C .

and FM order is even not present in the monolayer⁹. As a contrast, the FM exchange with an itinerant character mediated by carriers in metallic Fe_3GeTe_2 monolayer is much stronger than the superexchange in CrI_3 and $\text{Cr}_2\text{Ge}_2\text{Te}_6$, thus yielding a remarkably higher T_C of about ~ 130 K, which can be raised even above room temperature by using the ionic gating technique^{18,19}.

The tremendous efforts in perusing high T_C magnets more recently led to the discovery of a T_C of ~ 130 – 230 K in the bulk quasi-2D vdW $\text{Fe}_{3-x}\text{GeTe}_2$, which can even be enhanced up to room temperature¹⁸. Interestingly, similar as $\text{Fe}_{3-x}\text{GeTe}_2$, bulk $\text{Fe}_{5-x}\text{GeTe}_2$ shows a tunable T_C ranging from ~ 270 to ~ 363 K by controlling the Fe deficiency content x or by substituting Co for Fe, suggesting the detrimental role of Fe in the magnetic exchange^{20,21,56}. A reversible magnetoelastic coupled first-order transition near 100 K was detected by neutron powder diffraction²⁰. Considering the exotic physical properties in exfoliated Fe_3GeTe_2 nanoflakes and its heterostructures, such as the extremely large anomalous Hall effect²², planar topological Hall effect²³, Kondo lattice physics²⁴, anisotropic magnetostriction effect²⁵, spin filtered tunneling effect¹⁶, magnetic skyrmions²⁶, etc., Fe_5GeTe_2 would also be expected to provide extraordinary opportunities to explore intriguing physical properties. To well understand the physical properties of Fe_5GeTe_2 , the magnetic exchange model should be established first. However, the direct measurements on the magnetic structure are absent yet. Alternatively, study on the magnetic critical behavior and analysis of the critical exponents in vicinity of the paramagnetic (PM) to FM transition region could yield valuable insights into the magnetic exchange and properties. For example, the method has established the magnetic exchange models for CrI_3 ²⁷, VI_3 ²⁸, Fe_3GeTe_2 ^{29,30}, Co_2TiSe_2 ³¹, and $\text{Fe}_{0.26}\text{TaS}_2$ ³², etc. In this work, we have reported the investigation on the critical behavior of Fe_5GeTe_2 , which finds that the obtained set of critical exponents are close to those calculated from the renormalization group approach for a long-range 3D Heisenberg model with the magnetic exchange distance decaying as $J(r) \approx r^{-4.916}$.

Result and discussion

Characterizations on the crystal structure, quality and compositions are presented in the supplementary materials (SI). Figure 1a depicts the temperature dependence of magnetization $M(T)$ for Fe_3GeTe_2 , measured with zero-field-cooling (ZFC) and field-cooling (FC) mode under the applied magnetic field $H = 1$ kOe along the ab -plane of the crystal. The magnetization displays an abrupt PM to FM transition at ~ 270 K and no clear separation between the ZFC and FC curves. The inset of Fig. 1a is the inverse temperature dependent magnetic susceptibility $\chi^{-1}(T)$ with the dotted straight line representing the Curie–Weiss law fitting. It shows a deviation of $\chi^{-1}(T)$ from the straight line near 295 K which is much higher than T_C . The obtained Weiss temperature is 283 K, which is also

higher than T_C , indicating a strong FM interaction. The effective moment as $\mu_{\text{eff}} = 6.659 \mu_B/\text{Fe}$ is also obtained. Considering the varied effective magnetic moment of Fe^{2+} with the values ranging from 4.90 to 6.70 μ_B in various materials including sphalerite and monoclinic pyroxenes obtained from magnetic susceptibility analysis³³ and the Fe deficiency in our crystals, the value we obtained from the Curie–Weiss law fitting is reasonable. The FM ground state can also be demonstrated by the isothermal magnetization $M(H)$ shown in Fig. 1b measured at 2 K. The low coercive field indicates a soft ferromagnetism in Fe_5GeTe_2 , which is similar as that of Fe_3GeTe_2 ^{29,30}. The saturation magnetic moment along the c -axis is about 2.4 μ_B/Fe , likely unveiling the magnetic anisotropy at low temperature. The initial isothermal magnetizations in the temperature range of 261–285 K measured with $H//c$ -axis were shown in Fig. 1c and the Arrott plot³⁴, that is, M^2 vs. H/M , is shown in Fig. 1d. The positive slope of all M^2 vs. H/M curves, according to the Banerjee's criterion³⁵, indicates that the PM to FM transition has a second-order in nature. The Arrott plot was initially tried to for the analysis of the measured magnetizations, so the mean Landau mean-field theory with the critical exponents $\beta = 0.5$ and $\gamma = 1.0$ is involved. If it works, the M^2 vs. H/M curves should be straight and parallel to each other in the high magnetic field region, and additionally, the isothermal magnetization at T_C should pass through the origin. However, seen in Fig. 1d M^2 vs. H/M curves are clearly nonlinear with a downward curvature, suggesting that the fit does not work for Fe_5GeTe_2 . The failure of the Arrott plot within the framework of Landau mean-field theory lies in that the itinerant ferromagnetism in Fe_5GeTe_2 should have significant electronic correlations and spin fluctuations, which however are neglected in the Landau mean-field theory.

The second-order PM to FM phase transition in Fe_5GeTe_2 can be described by the magnetic equation of state and is characterized by critical exponents β , γ and δ that are mutually related. According to the scaling hypothesis, for a second-order phase transition, the spontaneous magnetization $M_S(T)$ below T_C , the inverse initial susceptibility $\chi_0^{-1}(T)$ above T_C and the magnetization M at T_C can be used to obtain β , γ and δ by using the equations³⁶:

$$M_S(T) = M_0(-\varepsilon)^\beta, \varepsilon < 0, T < T_C, \quad (1)$$

$$\chi_0^{-1}(T) = (h_0/m_0)\varepsilon^\gamma, \varepsilon > 0, T > T_C, \quad (2)$$

$$\text{and } M = DH^{1/\delta}, \varepsilon = 0, T = T_C, \quad (3)$$

where $\varepsilon = (T - T_C)/T_C$ is the reduced temperature, and M_0 , h_0/m_0 , and D are the critical amplitudes. Though the Landau mean-field theory can not be used, the critical isothermal magnetizations, alternatively, can be analyzed with the Arrott-Noakes equation of state³⁷:

$$(H/M)^{1/\gamma} = a\varepsilon + bM^{1/\beta}, \quad (4)$$

where a and b are the fitting constants. Five different models including the 2D Ising model ($\beta = 0.125$, $\gamma = 1.75$)³⁸, the 3D Heisenberg model ($\beta = 0.365$, $\gamma = 1.386$)³⁸, the 3D Ising model ($\beta = 0.325$, $\gamma = 1.24$)³⁸, the 3D XY model ($\beta = 0.345$, $\gamma = 1.316$)³⁹ and the tricritical mean-field model ($\beta = 0.25$, $\gamma = 1.0$)⁴⁰ were used for the modified Arrott plots, which are shown in Fig. 2a–e. One can see that the lines in Fig. 2d,e are not parallel to each other, thus excluding the tricritical mean-field and 2D Ising models. In Fig. 2a–c, all lines in each figure are almost parallel to each other in the high magnetic field region, thus making the choice of an appropriate model for Fe_5GeTe_2 impossible in this step. As we mentioned above, the modified Arrott plot should be a set of parallel lines in the high magnetic field region with the same slope of $S(T) = dM^{1/\beta}/d(H/M)^{1/\gamma}$. The normalized slope NS is defined by $NS = S(T)/S(T_C)$, which enables us an easy comparison of the NS of different models and to select out the most appropriate one with the ideal value of unity. The NS values versus the temperature for different models are plotted in Fig. 2f, which clearly show that the NS of the 2D Ising model has the largest deviation from unity. One can see that when $T > T_C$, NS of the 3D Ising model is close to unity, while when $T < T_C$ the 3D XY model seems as the best. This indicates that the critical behavior of Fe_5GeTe_2 may not belong to a single universality class. The fact also likely indicates that the magnetic character of Fe_5GeTe_2 is nearly isotropic above T_C and the enhancement of the anisotropic exchange below T_C .

To achieve in-depth insights into the nature of the PM to FM transition in Fe_5GeTe_2 , the precise critical exponents and critical temperature should be obtained. In the modified Arrott plot, the linear extrapolation of the nearly straight curves from the high magnetic field region intercepting the $M^{1/\beta}$ and $(H/M)^{1/\gamma}$ axes yields reliable values of $M_S(T)$ and $\chi_0^{-1}(T)$, respectively. The extracted $M_S(T)$ and $\chi_0^{-1}(T)$ can be used to fit the β and γ by using Eqs. (1) and (2). The thus obtained β and γ are thereafter used to reconstruct a modified Arrott plot. Consequently, new $M_S(T)$ and $\chi_0^{-1}(T)$ are generated from the linear extrapolation in the high field region, and a new set of β and γ will be acquired. This procedure should be repeated until β and γ are convergent. The obtained critical exponents from this method are independent on the initial parameters, thus guaranteeing the reliability of the analysis and that the obtained critical exponents are intrinsic. The final modified Arrott plot with $\beta = 0.351(1)$ and $\gamma = 1.413(5)$ is presented in Fig. 3, which shows that the isotherms in the high magnetic field region are actually a set of parallel straight lines. In addition, the final $M_S(T)$ and $\chi_0^{-1}(T)$ with solid fitting curves are depicted in Fig. 4a, which yield the critical exponents $\beta = 0.344(5)$ with $T_C = 273.76(3)$ K and $\gamma = 1.406(1)$ with $T_C = 273.88(4)$ K.

It is necessary to check the accuracy of above analysis. The Kouvel–Fisher (K-F) method can also be employed to fit the critical exponents and critical temperature, which is expressed as⁴⁰:

$$\frac{M_S(T)}{dM_S(T)/dT} = \frac{T - T_C}{\beta} \quad (5)$$

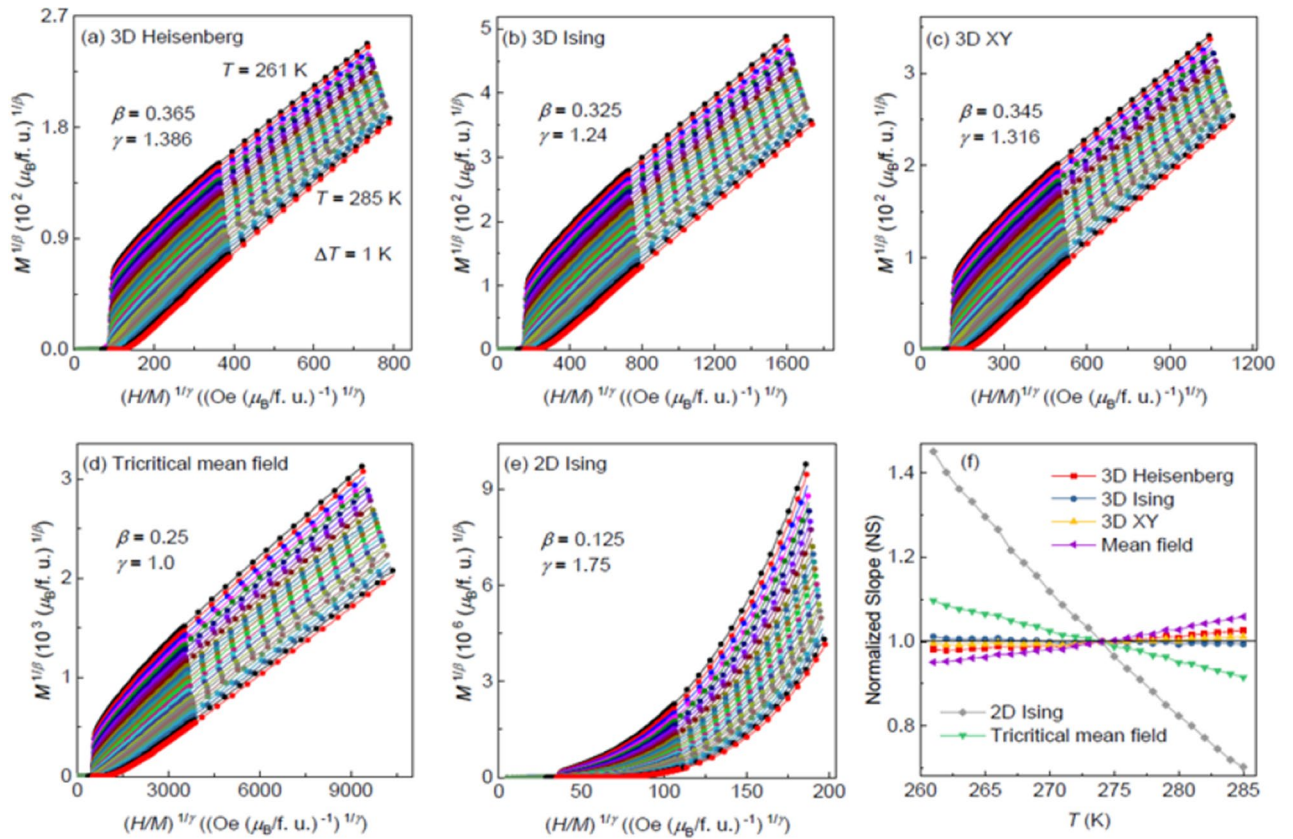


Figure 2. The isotherms of $M^{1/\beta}$ versus $(H/M)^{1/\gamma}$ with (a) 3D Heisenberg model, (b) 3D Ising model, (c) 3D XY model, (d) Tricritical mean-field model and (e) 2D Ising model. (f) Normalized slope versus temperature curves for six sets of critical exponents.

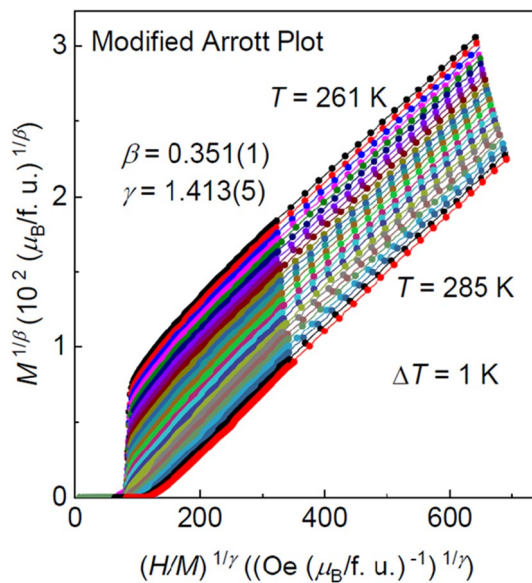


Figure 3. Modified Arrott plot of isotherms with $\beta=0.351(1)$ and $\gamma=1.413(5)$ for Fe_5GeTe_2 .

$$\text{and } \frac{\chi_0^{-1}(T)}{d\chi_0^{-1}(T)/dT} = \frac{T - T_C}{\gamma}, \tag{6}$$

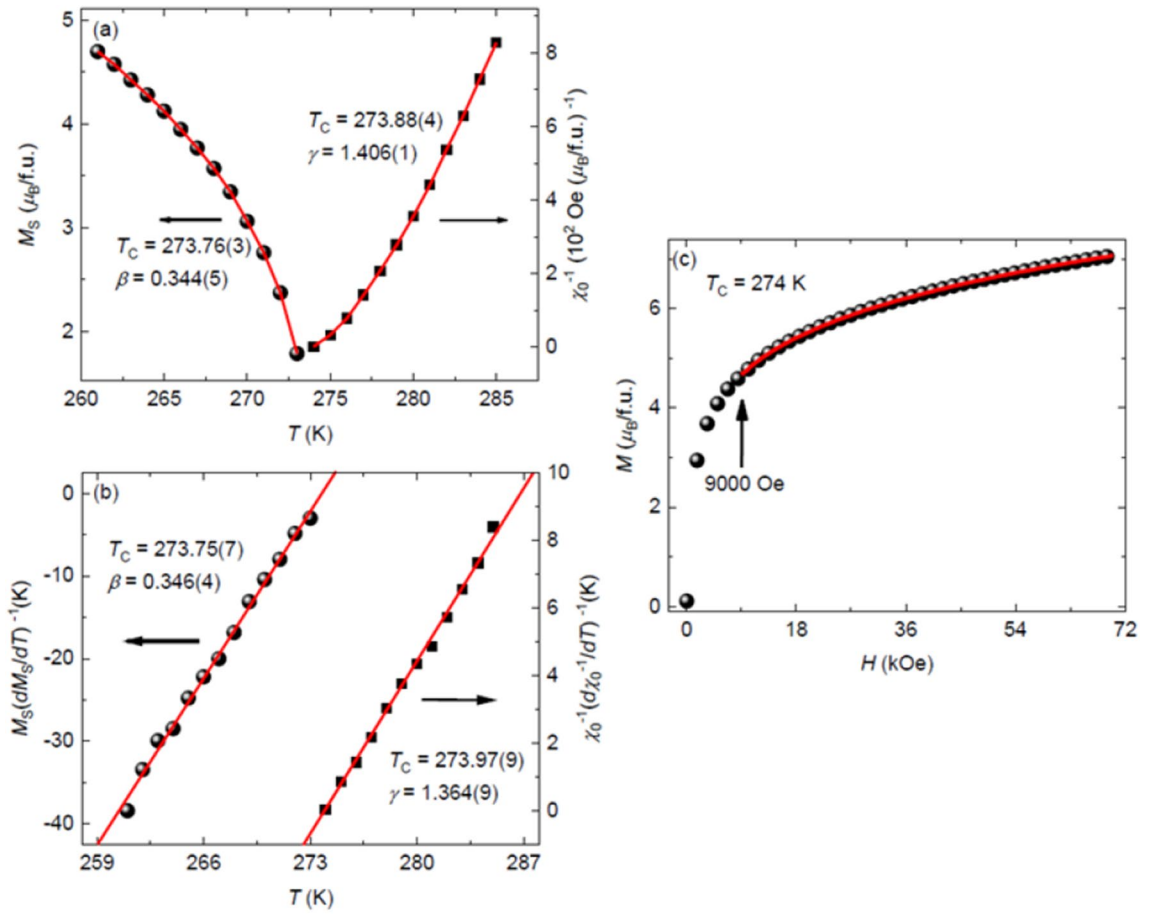


Figure 4. (a) Temperature dependence of the spontaneous magnetization M_S (left) and the inverse initial susceptibility $\chi_0^{-1}(T)$ (right) with solid fitting curves for Fe_5GeTe_2 . (b) Kouvel-Fisher plots of $M_S(T)/(dM_S(T)/dT)$ (left) and $\chi_0^{-1}(T)/(d\chi_0^{-1}(T)/dT)$ (right) with solid fitting curves for Fe_5GeTe_2 . (c) Isothermal $M(H)$ collected at $T_C = 274$ K for Fe_5GeTe_2 . Inset: the same plot in log–log scale with a solid fitting curve.

where $M_S(T)/(dM_S(T)/dT)$ and $\chi_0^{-1}(T)/(d\chi_0^{-1}(T)/dT)$ are linearly dependent on temperature with the slopes of $1/\beta$ and $1/\gamma$, respectively. As is shown in Fig. 4b, the linear fits give $\beta = 0.346(4)$ with $T_C = 273.75(7)$ K and $\gamma = 1.364(9)$ with $T_C = 273.97(9)$ K, respectively, which are consistent with those obtained from the iterative modified Arrott plot, thus confirming the reliability of the above analysis.

The iterative modified Arrott plot gives the critical exponents β and γ , while the critical exponent δ can be obtained by using Eq. (3). Figure 4c shows the isothermal magnetization $M(H)$ at a critical temperature $T_C = 274$ K and the inset shows the plot at a log–log scale. According to Eq. (3), the $M(H)$ at T_C should be a straight line in the log–log scale with the slope of $1/\delta$, thus giving $\delta = 5.02(1)$. To check the reliability of such analysis, δ was also calculated by using the Widom scaling relation⁴¹:

$$\delta = 1 + \frac{\gamma}{\beta}, \tag{7}$$

which gives $\delta = 5.02(6)$ and $\delta = 4.94(0)$ by using the β and γ obtained with modified Arrott plot and Kouvel-Fisher plot, respectively, which are consistent with those fitted by using Eq. (3).

From above analysis, a set of critical exponents are obtained, which are actually self consistent. It is of essential importance to check whether the obtained critical exponents and T_C can generate a scaling equation of state for Fe_5GeTe_2 , i.e., to examine the reliability of these critical exponents again by using the scaling analysis. According to the scaling hypothesis, for a magnetic system in the critical asymptotic region, the scaling equation of state can be expressed as⁴²:

$$M(H, \varepsilon) = \varepsilon^\beta f_\pm\left(\frac{H}{\varepsilon^{\beta+\gamma}}\right) \tag{8}$$

where $M(H, \varepsilon)$, H , and T are variables; f_+ for $T > T_C$ and f_- for $T < T_C$ are the regular functions. Equation (8) can also be written as:

$$m = f_\pm(h), \tag{9}$$

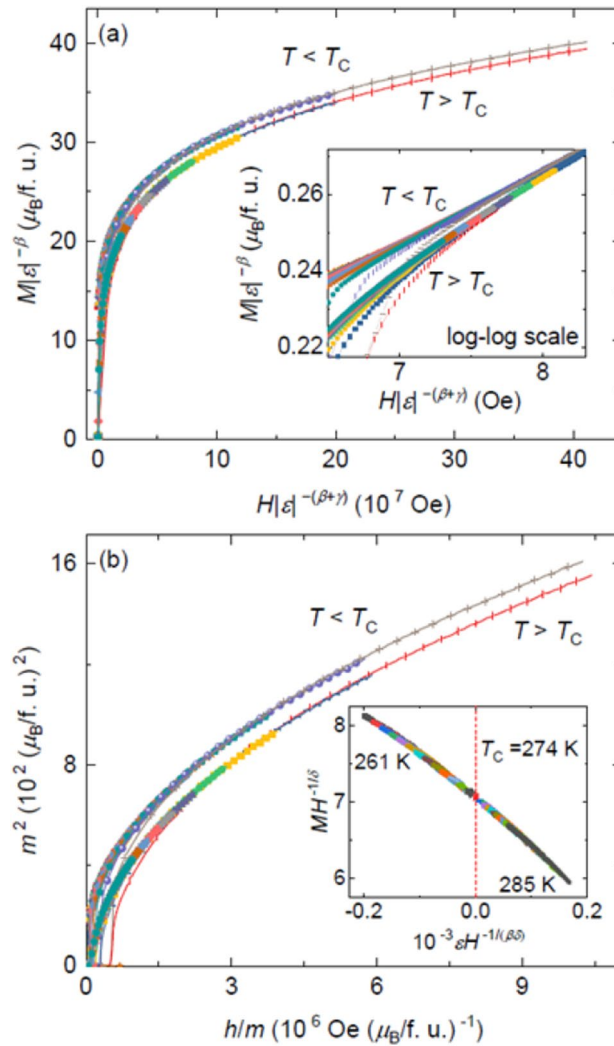


Figure 5. (a) The $m \equiv \varepsilon^{-\beta} M(H, \varepsilon)$ as a function of the $h \equiv \varepsilon^{-(\beta+\gamma)}$ below and above T_C for Fe_5GeTe_2 . Inset is the same $m(h)$ data in log–log scale. (b) Plot in the form of $m^2(h/m)$ for Fe_5GeTe_2 . Inset shows the plot of $\varepsilon H^{-(\beta\delta)}$ vs. $MH^{-1/\delta}$ below and above T_C .

where $m \equiv \varepsilon^{-\beta} M(H, \varepsilon)$ and $h \equiv \varepsilon^{-(\beta+\gamma)}$. If the critical exponents β , γ and δ could be properly chosen, the scaled $m(h)$ plot will fall onto two universal curves for $T > T_C$ and $T < T_C$, respectively. In such case, the interactions are believed to be properly renormalized in the critical regime following the scaling equation of state. The scaled m and h curves are plotted in Fig. 5a, which actually show two branches below and above T_C , thus guarantying the reliability of the obtained critical exponents. The two branches are much clear when the same data are plotted in a log–log form, seen by the inset of Fig. 5a. To support the analysis, we used a more rigorous method by plotting m^2 against h/m , seen in Fig. 5b in which all data apparently separate into two curves below and above T_C . The reliability of the obtained critical exponents and T_C can also be examined by checking the scaling of the magnetization curves. The scaling state equation of magnetic systems is⁴²:

$$\frac{H}{M^\delta} = h\left(\frac{\varepsilon}{H^{1/\beta}}\right), \tag{10}$$

where $h(x)$ is a scaling function. From Eq. (10), the $\varepsilon H^{-(\beta\delta)}$ vs. $MH^{-1/\delta}$ should fall on one universal curve⁴³, as seen by the inset of Fig. 5b. The T_C lies on the zero point of $\varepsilon H^{-(\beta\delta)}$ axis. As a result, the well rescaled curves further confirm that the obtained critical exponents and T_C are reliable and consistent with the scaling hypothesis.

It is valuable to compare the critical exponents of Fe_5GeTe_2 with those of other layered vdW magnets and those predicted by various models. The critical exponents of Fe_5GeTe_2 obtained by using different analysis techniques and different theoretical models are summarized in Table 1, together with those of other several FM vdW magnets including $\text{Fe}_{3-x}\text{GeTe}_2$ ($x = 0, 0.15, \text{ and } 0.36$), $\text{Cr}_2\text{Si}_2\text{Te}_6$, and $\text{Cr}_2\text{Ge}_2\text{Te}_6$. The previous comprehensive study reached a conclusion that the critical exponent β for a 2D magnets lies in the range of $\sim 0.1 \leq \beta \leq 0.25$ ⁴⁴. It is apparent that the β values of $\text{Cr}_2\text{Si}_2\text{Te}_6$ and $\text{Cr}_2\text{Ge}_2\text{Te}_6$, which were verified as 2D Ising magnets^{45,46}, are actually within the window, while those of $\text{Fe}_{3-x}\text{GeTe}_2$ and Fe_5GeTe_2 are apparently larger than 0.25, thus excluding

Composition	References	Technique	β	γ	δ	$\{d:n\}$	$J(r)$
Fe ₅ GeTe ₂	This work	MAP	0.351 (1)	1.413 (5)	5.02 (6)	{3:3}	$r^{-4.916}$
	This work	KF	0.346 (4)	1.364 (9)	4.94 (0)		
	This work	CI			5.02 (1)		
3D Heisenberg	⁴	Theory	0.365	1.386	4.8		
3D XY	⁴	Theory	0.345	1.316	4.81		
3D Ising	⁴	Theory	0.325	1.24	4.82		
Tricritical mean field	⁵	Theory	0.25	1.0	5		
Mean field	⁴	Theory	0.5	1.0	3		
Fe _{2.64} Ge _{0.87} Te ₂	¹²	KF	0.372 (4)	1.265 (1)	4.401 (6)	{3:3}	$r^{-4.89}$
Fe _{2.85} GeTe ₂	¹³	KF	0.363	1.228	4.398		$r^{-4.8}$
Fe ₃ GeTe ₂	³	KF	0.322 (4)	1.063 (8)	4.301 (6)		$r^{-4.6}$
Cr ₂ Si ₂ Te ₆	¹⁴	KF	0.175 (9)	1.562 (9)	9.925 (5)	{2:1}	$r^{-3.63}$
Cr ₂ Ge ₂ Te ₆	¹⁵	KF	0.200 (3)	1.28 (3)	7.405	{2:1}	$r^{-3.52}$

Table 1. A summary of the critical exponents of Fe₅GeTe₂, Fe_{3-x}GeTe₂, Cr₂Si₂Te₆, Cr₂Ge₂Te₆ and those predicted by different models (MAP: Modified Arrott plot; KF: Kouvel-Fisher method; CI: critical isotherm analysis).

d	n	σ	β	γ	δ
3	3	1.9160	0.3851	1.3613	4.5351
2	1	1.3603	0.3168	1.370	5.3241
2	3	1.2740	0.3904	1.370	4.5096

Table 2. Critical exponents calculated by the renormalization group theory.

the 2D Ising model for them^{29,30}. Moreover, the γ values of Fe_{3-x}GeTe₂ and Fe₅GeTe₂ are much larger than those for the tricritical mean-field and 3D Ising models^{38,39}, suggesting the two models are not appropriate. Combining the β and γ values, the magnetic critical behavior in Fe₅GeTe₂ should have a 3D nature, indicating that the interlayer magnetic exchange can not be neglected. It was suggested that Fe_{3-x}GeTe₂ has a smaller vdW gap and hence a stronger interlayer magnetic exchange than that in Cr₂(Si,Ge)₂Te₆¹⁷. It is therefore a natural hypothesis that the vdW gap in Fe₅GeTe₂ is also very small. To achieve more insights, the critical exponents of Fe₅GeTe₂ should be compared with the several 3D models more carefully. The β of Fe₅GeTe₂ is much closer to that of the 3D XY model³⁹ while the γ is closer to that of the 3D Heisenberg model³⁸, likely implying that the obtained critical exponents of Fe₅GeTe₂ can not be simply categorized into any conventional universality classes.

For a homogenous magnet, it is essential to use the magnetic exchange distance $J(r)$ to further determine the universality class of the magnetic phase transition. Within the framework of the renormalization group theory, the magnetic exchange decays with the distance r in a form $J(r) \sim e^{-r/b}$ for the short-range magnetic exchange and $J(r) \sim r^{-(d+\sigma)}$ for the long-range exchange, where r is the exchange distance, b is the spatial scaling factor, d is the dimensionality of the system, and the positive constant σ denotes the range of exchange interaction^{47,48}. Moreover, within this theory model the magnetic susceptibility exponent γ is defined as⁴⁷:

$$\gamma = 1 + \frac{4}{d} \left(\frac{n+2}{n+8} \right) \Delta\sigma + \frac{8(n+2)(n-4)}{d^2(n+8)^2} \left[1 + \frac{2G(\frac{d}{2})(7n+20)}{(n-4)(n+8)} \right] \Delta\sigma^2, \quad (11)$$

where n is the spin dimensionality, $\Delta\sigma = (\sigma - d/2)$ and $G(\frac{d}{2}) = 3 - \frac{1}{4}(\frac{d}{2})^2$. For 3D materials ($d=3$) with $3/2 \leq \sigma \leq 2$, the magnetic exchange decays relatively slowly as $J(r) \sim r^{-(d+\sigma)}$ due to a long-range magnetic exchange. For $\sigma > 2$, the 3D Heisenberg model is valid for 3D isotropic magnets, where $J(r)$ decreases faster than r^{-5} due to the short-range magnetic exchange, while when $\sigma \leq 3/2$, the mean-field model works and $J(r)$ decreases slower than r^{-4} ^{47,48}. To obtain the values of d , n , and σ for Fe₅GeTe₂, a method similar to that in Ref.⁴⁷ was adopted. In this method, σ is initially adjusted according to Eq. (11) with several sets of $\{d:n\}$ to get a proper γ that is close to the experimental value (~ 1.364). The obtained σ is then used to calculate other critical exponents by the following equations: $v = \gamma/\sigma$, $\alpha = 2 - vd$, $\beta = (2 - \alpha - \gamma)$, and $\delta = 1 + \gamma/\beta$. Several sets of $\{d:n\}$ will be tried, with the typical results being summarized Table 2, which finally achieved the critical exponents of $\beta = 0.3851$, $\gamma = 1.3613$ and $\delta = 4.5351$, which match well with the experimental values, when $\{d:n\} = \{3:3\}$ and $\sigma = 1.916$. Such a result indicates that the 3D Heisenberg type magnetic exchange with long-range interaction decaying as $J(r) \approx r^{-4.916}$ can account for the magnetic properties of Fe₅GeTe₂, which is consistent with our analysis presented above.

The magnetic exchange in quasi-2D vdW magnets has been subjected to immense investigations. For Cr₂Si₂Te₆, the magnetic critical behavior analysis and neutron scattering studies consistently suggest the universality class of 2D Ising model accounting for its magnetic properties^{26,49}. Because of the smaller vdW gap

and hence an enhanced interlayer exchange in $\text{Cr}_2\text{Ge}_2\text{Te}_6$, its critical behavior shows a transition from the 2D Ising-type to a 3D tricritical mean-field type⁵⁰. It is useful to compare the magnetic critical behavior of Fe_5GeTe_2 with that of Fe_3GeTe_2 . The mean distance between the two adjacent Te layers that across the vdW gap in Fe_3GeTe_2 is 0.423 nm⁵¹, which is rather close to that of CrGeTe_3 , 0.377 nm⁴⁹, which presumably can account for the 3D Heisenberg characteristics of the critical behavior. Previous studies on Fe_5GeTe_2 indicate small magnetic anisotropy at high temperature²⁰, so the 3D magnetism for the critical behavior in Fe_5GeTe_2 is reasonable. Moreover, it is found that the magnetic anisotropy in $\text{Fe}_{3-x}\text{GeTe}_2$ strongly depends on the Fe deficiency⁵², which can be largely suppressed with increasing the deficiency content x . If we pay a close attention to the critical exponents of Fe_5GeTe_2 , it is easily found that they are much closer to those of Fe deficient $\text{Fe}_{3-x}\text{GeTe}_2$ ²⁹, likely further demonstrating the weak magnetic anisotropy in Fe_5GeTe_2 . However, the possible transition between different universality classes of models of the critical behavior should be carefully checked, if we recall into our mind that a critical phase transition between 3 and 2D at the temperature of $\sim 0.9T_C$ in NiPS_3 and an anisotropic 2D to 3D magnetism below T_C in MnPS_3 were experimentally confirmed^{53,54}. Though such possibility has not been examined yet in $\text{Fe}_{3-x}\text{GeTe}_2$, considering that $\text{Fe}_{3-x}\text{GeTe}_2$ indeed shares similarities as MPS_3 ($M = \text{Mn, Fe, and Ni}$) in that they all have 2D antiferromagnetic ground state with the ferromagnetic layers in them order antiferromagnetically along the c -axis at low temperature, as well as the 3D critical behavior near T_C , the critical phase transition definitely need to be checked in $\text{Fe}_{3-x}\text{GeTe}_2$. For Fe_5GeTe_2 , it is somewhat different from MPS_3 and $\text{Fe}_{3-x}\text{GeTe}_2$, which behaves as an easy-axis vdW ferromagnet with the magnetic moments preferring to align along the c -axis but with weak anisotropy at high temperature due to the easy polarization of moments and the interaction between the FM layers is still FM. However, the magnetism of Fe_5GeTe_2 is somewhat complex due to the multiple Fe sublattices and composition tunable T_C . It is revealed that the magnetic moments on Fe(1) sublattice order below $\sim 100\text{--}120\text{ K}$ while the majority of the moments order at T_C ²¹. Short-range order associated with occupations of split sites of Fe(1) is also present. Additionally, the magnetic anisotropy is enhanced at low temperature. Regarding these, more studies to establish the precise spin structure at low temperature are extremely desired.

Conclusion

In summary, we have investigated the magnetic critical behavior in vicinity of the PM to FM phase transition in the quasi-2D van der Waals ferromagnet Fe_5GeTe_2 which has a near room temperature T_C of approximately 270 K. The estimated critical exponents β , γ and δ values from the various techniques and theoretical models show nice consistence with each other and follow the scaling behavior well. The critical exponents suggest a second order phase transition and they do not belong to any single universality class of model, just lying between the 3D Heisenberg model and the 3D XY model. The magnetic exchange distance is found to decay as $J(r) \approx r^{-4.916}$, which is close to that of 3D Heisenberg model with long-range exchange. The critical phenomena indicate weak magnetic anisotropy of Fe_5GeTe_2 at high temperature, possibly due to its small vdW gap. The very recent calculations indicate that monolayer formation energy of Fe_5GeTe_2 lies inside the energy range of other 2D materials⁵⁵, and the synthesis of the monolayer is therefore highly expected. Moreover, considering the tunable T_C which can even to be $\sim 350\text{ K}$ ^{20,21,56}, the investigation on the precise magnetic structure of Fe_5GeTe_2 would find extraordinary opportunities for applications in next-generation spintronic devices.

Methods

Single crystals were grown from chemical vapor transport (CVT) technique by using iodine as the transport agent, similar as the method described previously^{20,21}. The crystal used in this experiment is flat with a typical dimension of 2 mm * 2 mm * 0.1 mm. The crystallographic phase and crystal quality were examined on a Bruker D8 single crystal X-ray diffractometer (SXRD) with $\text{Mo K}\alpha$ ($\lambda = 0.71073\text{ \AA}$) at 300 K. The chemical compositions and uniformity of stoichiometry were checked by the energy dispersive spectroscopy (EDS) at several spots on the crystals. The direct current (dc) magnetization was measured on the Quantum Design magnetic properties measurement system (MPMS-3) with the magnetic field applied parallel to c -axis of the crystal. Isothermal magnetizations were collected at a temperature interval of 1 K in the temperature range of 261–285 K, which is just around T_C ($\sim 270\text{ K}$). It should be noted that each curve was initially magnetized. The applied magnetic field was corrected by considering the demagnetization factor, which was used for the analysis of critical behavior. The demagnetization factor is roughly estimated to be ~ 0.88 with considering the crystal size⁵⁷.

Received: 16 April 2020; Accepted: 27 August 2020

Published online: 18 September 2020

References

- Novoselov, K. S. *et al.* Electric field effect in atomically thin carbon films. *Science* **306**, 666–669 (2004).
- Zhang, Y., Tan, Y.-W., Stormer, H. L. & Kim, P. Experimental observation of the quantum Hall effect and Berry's phase in graphene. *Nature* **438**, 201–204 (2005).
- Mak, K. F., Lee, C., Hone, J., Shan, J. & Heinz, T. F. Atomically thin MoS_2 : A new direct-gap semiconductor. *Phys. Rev. Lett.* **105**, 136805 (2010).
- Lu, J. M. *et al.* Evidence for two-dimensional Ising superconductivity in gated MoS_2 . *Science* **350**, 1353–1357 (2015).
- Xi, X. *et al.* Strongly enhanced charge-density-wave order in monolayer NbSe_2 . *Nature Nanotechnol.* **10**, 765–769 (2015).
- Li, L. *et al.* Controlling many-body states by the electric-field effect in a two-dimensional material. *Nature* **529**, 185–189 (2016).
- Mermin, N. D. & Wagner, H. Absence of ferromagnetism or antiferromagnetism in one- or two-dimensional isotropic Heisenberg models. *Phys. Rev. Lett.* **17**, 1133 (1966).
- Huang, B. *et al.* Layer-dependent ferromagnetism in a van der Waals crystal down to the monolayer limit. *Nature* **546**, 270–273 (2017).

9. Gong, C. *et al.* Discovery of intrinsic ferromagnetism in two-dimensional van der Waals crystals. *Nature* **546**, 265–269 (2017).
10. Lin, M.-W. *et al.* Ultrathin nanosheets of CrSiTe₃: A semiconducting two-dimensional ferromagnetic material. *J. Mater. Chem. C* **4**, 315–322 (2016).
11. Bonilla, M. *et al.* Strong room-temperature ferromagnetism in VSe₂ monolayers on van der Waals substrates. *Nat. Nanotechnol.* **13**, 289–293 (2018).
12. O'Hara, D. J. *et al.* Room temperature intrinsic ferromagnetism in epitaxial manganese selenide films in the monolayer limit. *Nano Lett.* **18**, 3125–3133 (2018).
13. Wang, X. *et al.* Current-driven magnetization switching in a van der Waals ferromagnet Fe₃GeTe₂. *Sci. Adv.* **5**, eaaw8904 (2019).
14. Zhong, D. *et al.* Van der Waals engineering of ferromagnetic semiconductor heterostructures for spin and valleytronics. *Sci. Adv.* **3**, e1603113 (2017).
15. Samarth, N. Magnetism in flatland. *Nature* **546**, 216–217 (2017).
16. Song, T. C. *et al.* Giant tunneling magnetoresistance in spin-filter van der Waals heterostructures. *Science* **360**, 1214–1218 (2018).
17. McGuire, M. A., Dixit, H., Cooper, V. R. & Sales, B. C. Coupling of crystal structure and magnetism in the layered, ferromagnetic insulator CrI₃. *Chem. Mater.* **27**, 612–620 (2015).
18. Deng, Y. *et al.* Gate-tunable room-temperature ferromagnetism in two-dimensional Fe₃GeTe₂. *Nature* **563**, 94–99 (2018).
19. Li, Q. *et al.* Patterning-induced ferromagnetism of Fe₃GeTe₂ van der Waals materials beyond room temperature. *Nano Lett.* **18**, 5974–5980 (2018).
20. May, A. F. *et al.* Ferromagnetism near room temperature in the cleavable van der Waals crystal Fe₃GeTe₂. *ACS Nano* **13**, 4436–4442 (2019).
21. May, A. F., Bridges, C. A. & McGuire, M. A. Physical properties and thermal stability of Fe_{3-x}GeTe₂ single crystals. *Phys. Rev. Mater.* **3**, 104401 (2019).
22. Kim, K. *et al.* Large anomalous Hall current induced by topological nodal lines in a ferromagnetic van der Waals semimetal. *Nat. Mater.* **17**, 794–799 (2018).
23. You, Y. *et al.* Planar topological Hall effect in a uniaxial van der Waals ferromagnet Fe₃GeTe₂. *Phys. Rev. B* **100**, 134441 (2019).
24. Zhang, Y. *et al.* Emergence of Kondo lattice behavior in a van der Waals itinerant ferromagnet, Fe₃GeTe₂. *Sci. Adv.* **4**, eaao6791 (2018).
25. Zhuang, H. L., Kent, P. R. C. & Hennig, R. G. Strong anisotropy and magnetostriction in the two-dimensional Stoner ferromagnet Fe₃GeTe₂. *Phys. Rev. B* **93**, 134407 (2016).
26. Ding, B. *et al.* Observation of magnetic Skyrmion Bubbles in a van der Waals ferromagnet Fe₃GeTe₂. *Nano Lett.* **20**, 868–873 (2020).
27. Liu, Y. & Petrovic, C. Three-dimensional magnetic critical behavior in CrI₃. *Phys. Rev. B* **97**, 014420 (2018).
28. Liu, Y., Abeykoon, M. & Petrovic, C. Critical behavior and magnetocaloric effect in VI₃. *Phys. Rev. Res.* **2**, 013013 (2020).
29. Liu, Y., Ivanovski, V. N. & Petrovic, C. Critical behavior of the van der Waals bonded ferromagnet Fe_{3-x}GeTe₂. *Phys. Rev. B* **96**, 144429 (2017).
30. Liu, B. J. *et al.* Critical behavior of the van der Waals bonded high T_C ferromagnet Fe₃GeTe₂. *Sci. Rep.* **7**, 6184 (2017).
31. Rahman, A. *et al.* Critical behavior in the half-metallic Heusler alloy Co₂TiSn. *Phys. Rev. B* **100**, 214419 (2019).
32. Zhang, C. H. *et al.* Critical behavior of intercalated quasi-van der Waals ferromagnet Fe_{0.26}TaS₂. *Phys. Rev. Mater.* **3**, 114403 (2019).
33. Parks, G. A. & Akhtar, S. Magnetic moment of Fe²⁺ in paramagnetic minerals. *Am. Mineralog. J. Earth Planet. Mater.* **53**, 406–415 (1968).
34. Arrott, A. Criterion for ferromagnetism from observations of magnetic isotherms. *Phys. Rev.* **108**, 1394–1396 (1957).
35. Banerjee, B. On a generalised approach to first and second order magnetic transitions. *Phys. Lett.* **12**, 16–17 (1964).
36. Fisher, M. E. The theory of equilibrium critical phenomenon. *Rep. Prog. Phys.* **30**, 615 (1967).
37. Arrott, A. & Noakes, J. E. Approximate equation of state for nickel near its critical temperature. *Phys. Rev. Lett.* **19**, 786 (1967).
38. Kaul, S. N. Static critical phenomenon in ferromagnets with quenched disorder. *J. Mag. Magn. Mater.* **53**, 5–53 (1985).
39. Le Guillou, J. C. & Zinn-Justin, J. Critical exponents from field theory. *Phys. Rev. B* **21**, 3976 (1980).
40. Kouvel, J. S. & Fisher, M. E. Detailed magnetic behavior of nickel near its curie point. *Phys. Rev.* **136**, A1626–A1632 (1964).
41. Widom, B. Surface tension and molecular correlations near the critical point. *J. Chem. Phys.* **43**, 3892 (1965).
42. Stanley, H. E. *Phase Transitions and Critical Phenomena* (Clarendon Press, Oxford., 1971).
43. Phan, M. *et al.* Tricritical point and critical exponents of La_{0.7}Ca_{0.3-x}Sr_xMnO₃ (x = 0, 0.05, 0.1, 0.2, 0.25) single crystals. *J. Alloy. Comp.* **508**, 238–244 (2010).
44. Taroni, A., Bramwell, S. T. & Holdsworth, P. C. Universal window for two-dimensional critical exponents. *J. Phys. Condens. Matter.* **20**, 275233 (2008).
45. Liu, Y. & Petrovic, C. Critical behavior of quasi-two-dimensional semiconducting ferromagnet Cr₂Ge₂Te₆. *Phys. Rev. B* **96**, 054406 (2017).
46. Liu, B. *et al.* Critical behavior of the quasi-two-dimensional semiconducting ferromagnet CrSiTe₃. *Sci. Rep.* **6**, 33873 (2016).
47. Fisher, M. E., Ma, S.-K. & Nickel, B. Critical exponents for long-range interactions. *Phys. Rev. Lett.* **29**, 917–920 (1972).
48. Fisher, S., Kaul, S. N. & Kronmüller, H. Critical magnetic properties of disordered polycrystalline Cr₇₅Fe₂₅ and Cr₇₀Fe₃₀ alloys. *Phys. Rev. B* **65**, 064443 (2002).
49. Carteaux, V., Moussa, F. & Spiesser, M. 2D Ising-like ferromagnetic behaviour for the lamellar Cr₂Si₂Te₆ compound: A neutron scattering investigation. *Europhys. Lett.* **29**, 251–256 (1995).
50. Lin, G. T. *et al.* Tricritical behavior of the two-dimensional intrinsically ferromagnetic semiconductor CrGeTe₃. *Phys. Rev. B* **95**, 245212 (2017).
51. Ouvrard, G., Sandre, E. & Brec, R. Synthesis and crystal structure of a new layered phase: The chromium hexatellurosulfate Cr₂Si₂Te₆. *J. Solid State Chem.* **73**, 27–32 (1988).
52. May, A. F., Calder, S., Cantoni, C., Cao, H. & McGuire, M. A. Magnetic structure and phase stability of the van der Waals bonded ferromagnet Fe_{3-x}GeTe₂. *Phys. Rev. B* **93**, 014411 (2016).
53. Wildes, A. R. *et al.* Magnetic structure of the quasi-two-dimensional antiferromagnet NiPS₃. *Phys. Rev. B* **92**, 224408 (2015).
54. Wildes, A. R. *et al.* Static and dynamic critical properties of the quasi-two-dimensional antiferromagnet MnPS₃. *Phys. Rev. B* **74**, 094422 (2006).
55. Joe, M., Yang, U. & Lee, C. First-principles study of ferromagnetic metal Fe₃GeTe₂. *Nano Mater. Sci.* **1**, 299–303 (2019).
56. Tian, C. K. *et al.* Tunable magnetic properties in van der Waals crystals (Fe_{1-x}Co_x)₃GeTe₂. *Appl. Phys. Lett.* **116**, 202402 (2020).
57. Chen, D. X., Pardo, E. & Sanchez, A. Demagnetizing factors of rectangular prisms and ellipsoids. *IEEE Trans. Magn.* **38**, 1742 (2002).

Acknowledgements

The authors acknowledge the support by the National Natural Science Foundation of China (Grant No. 11874264), Y.F.G. acknowledges the starting grant of ShanghaiTech University and the Program for Professor of Special Appointment (Shanghai Eastern Scholar). L.M.C. is supported by the Key Scientific Research Projects of Higher Institutions in Henan Province (19A140018). The authors also thank the support from the Analytical Instrumentation Center (#SPST-AIC10112914), SPST, ShanghaiTech University.

Author contributions

Y.F.G. conceived and planned the experimental project. Z.X.L. grew the crystals with the help from W. X. and Y.P.F. Z.X.L. measured the magnetization assisted by H.S., X.W. and Z.Q.Z. Z.X.L., Z.H.Y. and N.Y. contributed to single crystal x-ray diffraction characterizations on the structure and quality of the crystals. Z.X.L. analyzed the data with help from L.M.C. Y.F.G., Z.X.L. and L.M.C. wrote the paper with inputs from all coauthors. All authors discussed the results and commented on the manuscript.

Competing interests

The authors declare no competing interests.

Additional information

Supplementary information is available for this paper at <https://doi.org/10.1038/s41598-020-72203-3>.

Correspondence and requests for materials should be addressed to L.C. or Y.G.

Reprints and permissions information is available at www.nature.com/reprints.

Publisher's note Springer Nature remains neutral with regard to jurisdictional claims in published maps and institutional affiliations.



Open Access This article is licensed under a Creative Commons Attribution 4.0 International License, which permits use, sharing, adaptation, distribution and reproduction in any medium or format, as long as you give appropriate credit to the original author(s) and the source, provide a link to the Creative Commons licence, and indicate if changes were made. The images or other third party material in this article are included in the article's Creative Commons licence, unless indicated otherwise in a credit line to the material. If material is not included in the article's Creative Commons licence and your intended use is not permitted by statutory regulation or exceeds the permitted use, you will need to obtain permission directly from the copyright holder. To view a copy of this licence, visit <http://creativecommons.org/licenses/by/4.0/>.

© The Author(s) 2020